Large-scale prediction of the parity distribution in the nuclear level density and application to astrophysical reaction rates

D. Mocelj,[1,*] T. Rauscher,[1,†] G. Martínez-Pinedo,[2] K. Langanke,[2,3]
L. Pacearescu,[4,‡] A. Faessler,[4] F.-K. Thielemann,[1] and Y. Alhassid[5]

[1] *Departement für Physik und Astronomie, Universität Basel, Basel, Switzerland*
[2] *GSI Darmstadt, Darmstadt, Germany*
[3] *Institut für Kernphysik, Technische Universität Darmstadt, Darmstadt, Germany*
[4] *Institut für Theoretische Physik, Universität Tübingen, Tübingen, Germany*
[5] *Center for Theoretical Physics, Sloane Physics Laboratory, Yale University, New Haven, CT, USA*

A generalized method to calculate the excitation-energy dependent parity ratio in the nuclear level density is presented, using the assumption of Poisson distributed independent quasi particles combined with BCS occupation numbers. It is found that it is crucial to employ a sufficiently large model space to allow excitations both from low-lying shells and to higher shells beyond a single major shell. Parity ratios are only found to equilibrate above at least 5–10 MeV of excitation energy. Furthermore, an overshooting effect close to major shells is found where the parity opposite to the ground state parity may dominate across a range of several MeV before the parity ratio finally equilibrates. The method is suited for large-scale calculations as needed, for example, in astrophysical applications. Parity distributions were computed for all nuclei from the proton dripline to the neutron dripline and from Ne up to Bi. These results were then used to recalculate astrophysical reaction rates in a Hauser-Feshbach statistical model. Although certain transitions can be considerably enhanced or suppressed, the impact on astrophysically relevant reactions remains limited, mainly due to the thermal population of target states in stellar reaction rates.

PACS numbers: 26.50.+x – 21.10.Ma – 24.60.Dr – 26.30.+k

I. INTRODUCTION

Knowledge of the nuclear level density in general and, more specifically, at low excitation energies is of interest for a number of reasons. Comparison to experimental level densities helps testing nuclear structure models [1]. In reaction theory, the nuclear level density is an important ingredient both for the determination of the relevant reaction mechanism and for the calculation of reaction cross sections [2]. Because of the low effective interaction energies in astrophysical applications, the level density at low excitation energy is usually assumed to be crucial to determine astrophysical reaction rates.

The level density ρ as a function of spin J, parity π, and excitation energy E can be written as

$$\rho\left(E,J,\pi\right)=\mathcal{P}\left(E,\pi\right)\mathcal{F}\left(E,J\right)\rho_{\mathrm{tot}}\left(E\right) \quad , \qquad (1)$$

with the spin projection $\mathcal{F}$. In most previous applications to astrophysics (e.g. [2]), equally distributed parities with $\mathcal{P}(E,\pi=\pm1)=1/2$ for both even and odd parity have been assumed at all energies but it is obvious that this assumption is not valid at low excitation energies. This work focuses on the determination of the parity projection factor $\mathcal{P}$ and its implication on the calculation of reaction rates for astrophysics.

In astrophysical applications usually different aspects are emphasized than in pure nuclear physics investigations. Explosive burning produces a large number of unstable nuclei for which experimental information is unavailable. Thus, the study of such models requires prediction of nuclear properties for a large number of nuclei, several thousands when considering all nucleosynthesis processes. On the other hand, reaction rates are obtained by energy-averaging cross sections in the relevant energy range (see Eq. 26), given by the so-called Gamow window [3]. Therefore, small deviations from the true cross sections may cancel out. This also may dampen the impact of variations in the predicted nuclear properties, such as the nuclear level density.

In principle, the nuclear level density should be extracted from microscopic models. However, conventional shell model calculations of level density are limited to the mass range $A \lesssim 50$ [4, 5, 6] because of the combinatorial increase of the dimension of the model space with the number of single-particle levels and/or the number of valence nucleons. Large-scale shell model calculations of level densities are possible in the framework of the shell model Monte Carlo (SMMC) method [7, 8, 9]. Most SMMC calculations have been carried out in one full major shell. However, they can be extended to higher excitation energies by including all other shells within a mean-field approximation [1]. The SMMC calculations are in general time-consuming and are difficult to carry out for the large number of nuclei required in large-scale astrophysical applications so far. Although computers have become faster, a consistent microscopic description of all required properties for all nuclei is still not feasi-

*Current address: ifb International AG, Pfäffikon, Switzerland
†Corresponding author
‡Current address: Deutsche Thomson-Brandt GmbH, Villingen Research Lab, Villingen, Germany

ble. This is, of course, also due to the still insufficient knowledge of nuclear interactions in general and its effects in neutron- or proton-rich nuclei. Therefore, many approaches for calculating astrophysical reaction rates make use of more phenomenological treatments. This does not imply that they are just mathematical fits to a given property, made in the region of stability and then extrapolated to unstable nuclei. Instead, they are based on some physical insight in the origin of the given property which makes it possible to extend its application also to unknown nuclei with only few parameters to be adapted. Among the traditional examples of such approaches is the shifted Fermi-gas model [10, 11] of the nuclear level density and its variations. As long as nucleons can be assumed to exhibit a Fermi-gas behavior, the energy dependence of the level density can be described by a few parameters. This has been proven repeatedly by comparison to experimental data but also in comparison to microscopic calculations [1, 12, 13, 14]. Also the behavior of its parameters can be determined by applying known physical facts and/or by extracting them from different types of calculations [2, 15]. Another example of the combined phenomenological approach is the macroscopic-microscopic Finite Range Droplet Model (FRDM) [16] which still proves to be the most successful model to predict nuclear masses.

In the spirit of the above we present a macroscopic-microscopic method to determine the parity ratio of nuclear levels from low to high excitation energy which can be easily applied to a large number of nuclei. Providing the factor $\mathcal{P}$ as a function of excitation energy – as we do in the following – has the additional advantage that it can be combined with any total level density $\rho_{\rm tot}$ from any other approach to determine the density of odd and even parity states. The method is based on a quasi-particle model proposed in Ref. [17] which we extend by allowing odd particle numbers, inclusion of all shells up to the 11 $\hbar\omega$ oscillator shell, and including excitations between all considered shells. Preliminary results were reported in [18, 19, 20, 21].

The method is introduced in Sec. II, with a discussion of some interesting effects found in the parity ratios included in Sec. II D. Sec. III then focusses on the astrophysical relevance of the parity distribution. Astrophysical rates computed with the new parity ratio are compared to standard rates widely used in astrophysical applications in Sec. III C. The paper is concluded with a summary in Sec. IV.

II. DETERMINATION OF PARITY RATIOS

A. Basic approach

We start from the assumption of statistically independent particles at finite temperature. Because single particle (s.p.) levels can either be occupied or empty, the probability distribution for the occupation can be assumed to be binomial [13]. The probability to occupy n out of r levels is therefore given by:

$$B(r;n) = \binom{r}{n} p^n (1-p)^{r-n}, \tag{2}$$

where the probability of occupying a level is denoted by p. We follow [17] by replacing the binomial distribution by a Poisson distribution $P(s)$. This approximation holds provided the number of levels r is large and the probability p is small, with the product rp finite. This can always be achieved by clustering the single particles into two groups according to their parity and counting only particles in the group having the opposite parity to the last occupied level. The probability to find n particles in that group is then

$$P(n) = \frac{f^n}{n!} e^{-f}, \tag{3}$$

where the average number of particles in the group is given by f. Obviously, neutrons and protons have to be treated separately. For an even number of nucleons the probability to find the whole system in a positive parity state is therefore given by

$$P^+ = \sum_{n,\text{even}} \frac{f^n}{n!} e^{-f} = \cosh f e^{-f}, \tag{4}$$

and to find the system in a negative parity state by

$$P^- = \sum_{n,\text{odd}} \frac{f^n}{n!} e^{-f} = \sinh f e^{-f}. \tag{5}$$

The probabilities can be related to the total partition function

$$Z = Z^+ + Z^- \tag{6}$$

and the partition functions for odd and even parity states, Z^- and Z^+, by

$$\begin{aligned} P^+ &= \frac{Z^+}{Z}, \\ P^- &= \frac{Z^-}{Z}. \end{aligned} \tag{7}$$

This leads to the expression used in [17] for even-even nuclei:

$$\frac{Z^-}{Z^+} = \tanh f. \tag{8}$$

It can be shown [22] that it can be completely generalized for even and odd numbers of particles by denoting the total ground state parity of a nucleus by g and the opposite parity by s:

$$\frac{P^s}{P^g} = \frac{Z^s}{Z^g} = \tanh f', \tag{9}$$

where $f' = f_{\rm n} + f_{\rm p}$ is now computed from the sum of the individual average particle numbers f of neutrons and protons.

In order to determine the desired parity factor $\mathcal{P}$ the ratio of the level densities ρ_g, ρ_s with different parity has to be known. Applying the well-known Laplace transform of the partition function and employing the saddle point approximation, the ratio for an excitation energy E is given by [22]

$$\frac{\rho_s}{\rho_g} = \frac{\beta^s}{\beta^g}\frac{Z^s}{Z^g}\sqrt{\frac{C^g}{C^s}}e^{(\beta^s-\beta^g)E} \ , \tag{10}$$

with the heat capacities C^g, C^s. In general, because of the different number of particles in each group, the inverse nuclear temperatures β^s, β^g will be different for the same excitation energy E. The required partition functions are determined by

$$\begin{aligned} Z^g &= \frac{1}{1+\tanh f'}, \\ Z^s &= \frac{1}{1+\frac{1}{\tanh f'}} \ . \end{aligned} \tag{11}$$

The thermal energy E and the heat capacities can be derived from the standard thermodynamic relations

$$\begin{aligned} E &= -\frac{\partial \ln Z}{\partial \beta} \\ C &= -\beta^2\frac{\partial^2 \ln Z}{\partial \beta^2} \ . \end{aligned} \tag{12}$$

Finally, the parity projection factor $\mathcal{P}$ is given by

$$\begin{aligned} \mathcal{P}(E,\pi=\pi_g) = \mathcal{P}_g &= \frac{\rho_g}{\rho_{\rm tot}} = \frac{1}{1+\xi}\,, \\ \mathcal{P}(E,\pi=\pi_s) = \mathcal{P}_s &= \frac{\rho_s}{\rho_{\rm tot}} = \frac{1}{1+\frac{1}{\xi}}\,, \end{aligned} \tag{13}$$

with

$$\xi = \frac{\rho_s}{\rho_g} \tag{14}$$

and π_g being the ground state parity of the nucleus while π_s being the opposite parity.

B. Determination of the mean occupation number

The central quantities $f_{\rm n}$, $f_{\rm p}$ were determined separately for neutrons and protons. In the following, we denote them by f for simplicity and imply that the two kinds of nucleons were treated separately with their respective s.p. levels and particle numbers. Assuming Fermi-Dirac distributed particles, the occupancy f_k of each s.p. level with energy ϵ_k given by

$$f_k^{FD} = \frac{1}{1+e^{\beta(\epsilon_k-\bar{\mu})}} \tag{15}$$

and the average number of particles by

$$\langle n \rangle = \sum_k f_k \ . \tag{16}$$

Proceeding as before by dividing the s.p. levels into a group exhibiting the same parity π_g as the last occupied state below the chemical potential $\bar{\mu}$ and another group with opposite parity π_s, the mean value f in the Poisson distribution is then given by

$$f = \sum_{k\in\pi_s} f_k^{FD} = \sum_{k\in\pi_s}\frac{1}{1+e^{\beta(\epsilon_k-\bar{\mu})}} \ . \tag{17}$$

The chemical potential is found iteratively from the particle number equation

$$n = \sum_k \frac{1}{1+e^{\beta(\epsilon_k-\bar{\mu})}} \quad . \tag{18}$$

With decreasing nuclear temperature $T_{\rm nuc}$ pairing interactions become increasingly important in nuclear systems, leading to nucleon pairs in the ground state and at low excitation energies. The breaking of such pairs requires additional energy. Hence, the Fermi-Dirac distribution will not be able to describe the occupation properly at high values of $\beta = 1/T_{\rm nuc}$. For example, this can be seen in Fig. 3 of [17] where a comparison between Fermi-Dirac and BCS occupancies and resulting partition ratios Z_-/Z_+ are shown for even-even nuclei. At high nuclear temperatures the microscopic distributions are well described by Fermi-Dirac statistics but for lower temperatures deviations start to appear. For those cases of even-even nuclei, the probability to find an even number of particles in the π_s parity group is clearly enhanced, odd numbers of particles are suppressed as seen in the comparison to the SMMC result in [17]. Similar effects were reported in [1].

Pairing effects can be included by using the well-known Bardeen-Cooper-Schrieffer (BCS) formalism [23], introducing the BCS occupancy for quasi-particles

$$f_k^{BCS} = 1/(1+\exp(\beta E_k)) \tag{19}$$

with the quasi-particle energy

$$E_k = \sqrt{(\epsilon_k-\bar{\mu})^2+\Delta^2} \ . \tag{20}$$

The chemical potential $\bar{\mu} = \bar{\mu}(\beta)$ and the pairing gap $\Delta = \Delta(\beta)$ are determined for each nuclear temperature $T_{\rm nuc} = 1/\beta$ by solving a non-linear system of equations, the well-known particle number and gap equation

$$\begin{aligned} n &= \frac{1}{2}\sum_k\left(1-\frac{\epsilon_k-\bar{\mu}}{E_k}\tanh\left(\frac{\beta}{2}E_k\right)\right) \\ \frac{2}{\Delta} &= \frac{G}{2}\sum_k\frac{\Delta}{E_k}\tanh\left(\frac{\beta}{2}E_k\right) \ , \end{aligned} \tag{21}$$

where G is the usual effective pairing coupling constant which determines the zero-temperature pairing gap Δ.

Although the single particles are no longer independent in the paired solution, the Poisson approach of Sec. II A can be kept, assuming that the quasi particles are statistically independent here. For the calculation of the mean occupation in the π^s parity group, it is sufficient to consider only contributions from quasi-particles, as condensed pairs do not contribute to any parity change of the system. This leads to

$$f = \sum_{k\in\pi_s} f_k^{BCS} = \sum_{k\in\pi_s} \frac{1}{1+\exp(\beta E_k)} \ . \qquad (22)$$

It should be noted that here the chemical potential $\bar{\mu}$ and the pairing gap Δ are temperature-dependent, i.e. have to be known as a function of β or $T_{\rm nuc}$. The BCS equations are solved iteratively for each inverse temperature β.

At sufficiently high nuclear temperature, pairing becomes negligible and there is a phase transition from the BCS to the Fermi-Dirac regime. However, this transition is not smooth when only using the above description because the BCS equations break down above a critical temperature $T_{\rm c} = 1/\beta_{\rm c}$. Due to the phase transition occuring at $T_{\rm c}$, the derivatives of the partition function Z (containing the mean occupancy f) are discontinuous when moving from the BCS regime to the Fermi-Dirac regime. This induces numerical problems in the solution of Eq. (10) via Eq. (12), especially also because the different parity groups exhibit different temperatures. To avoid the problematic temperature range would be too limiting because the range of excitation energies most interesting for studying the parity ratios would be excluded. Therefore, we employed an approximation by extrapolating the pairing gap to higher nuclear temperatures. In fact, the transition from the BCS to the Fermi-Dirac regime should be smooth in nuclei because the pair coherence length is much larger than the nuclear radius [24]. In such systems with dimensions smaller than the coherence length, fluctuations in the order parameters become important and wash out the discontinuity.

As the pairing effects vanish for high nuclear temperatures, the pairing gap itself should approach a value of Zero, thus recovering the Fermi-Dirac shape of the distribution (see, e.g., Ref. [25] for experimental indications of this effect). This behavior of the gap could be rigorously obtained, for instance, by using the static path approximation, integrating over the static fluctuations of the gap [26]. However, as has been shown in SMMC calculations [7, 27], this behavior can be simply parameterized in terms of a Fermi-type dependence:

$$\Delta^{\rm fit}(\beta) = \Delta^{\rm fit}(T_{\rm nuc}) = \Delta_T = \frac{\Delta_0}{1+\exp(-(T_{\rm nuc}-T'_{\rm nuc})/a)} \ , \qquad (23)$$

where Δ_0 denotes the pairing gap for $T_{\rm nuc} = 0$. The parameters $T'_{\rm nuc}$ and a were fitted so that the function approximated as closely as possible the behavior of the BCS gap below the critical temperature. As starting values we chose $T'_{\rm nuc} = 0.8T_{\rm c}$ and $a = (T'_{\rm nuc} - T_{\rm nuc})/\ln(\Delta_0/\Delta^{\rm BCS}_{T'_{\rm nuc}} - 1)$ which yielded a good fit to the BCS pairing gap

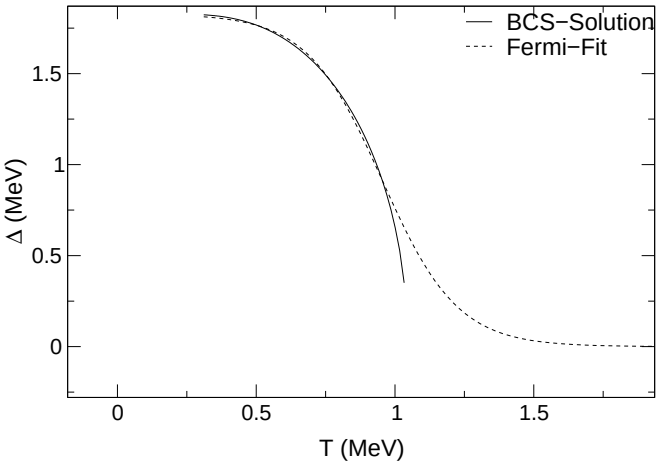

FIG. 1: Dependence on nuclear temperature of the proton pairing gap Δ in ^{66}Zn and its fit by a Fermi-type function (see text).

$\Delta^{\rm BCS} = \Delta$ below $T'_{\rm nuc}$. This results in a suppression of the pairing gap across a temperature range of the order of MeV, as also previously found in [7, 12, 27]. For illustration, Fig. 1 shows a comparison of the BCS solution and the fit for ^{66}Zn. The results are not sensitive to small variations in the choice of the starting values. These fits were subsequently used in the calculation of the chemical potential $\bar{\mu}$ and finally of the mean occupation number f by applying Eq. (22) for all values of β.

C. Input quantities and consistency

The parity projected partition functions Z^g, Z^s are related to each other, to the total partition function Z, and to the average occupancy f by Eqs. (6) and (9). Thus, the total partition function Z and the average occupation number f remain to be determined.

The determination of f as described in the previous section implicitly requires knowledge of the pairing strength G and the s.p. levels. For systems with an even number of particles, the starting value Δ_0 of the pairing gap was extracted from odd-even mass differences as described in [2]. This value was then used to determine the effective pairing strength G by solving the coupled Eqs. (21) for $T_{\rm nuc} = 0$. Further application of Eqs. (21) with fixed G at finite nuclear temperatures yields the temperature-dependence of Δ and the required occupation of quasi-particle states. Differently from the treatment of the pairing gap Δ_0 in [2], here we set $\Delta_0 = 0$ for systems with odd numbers of particles because the pairing effects are expected to be weak and quickly vanishing with increasing T_{nuc}. This means that a pure Fermi-Dirac distribution is used for odd particle numbers without the need to fit the phase transition.

The s.p. levels were calculated in a deformed Saxon-Woods potential [28] with parameters from [29] which

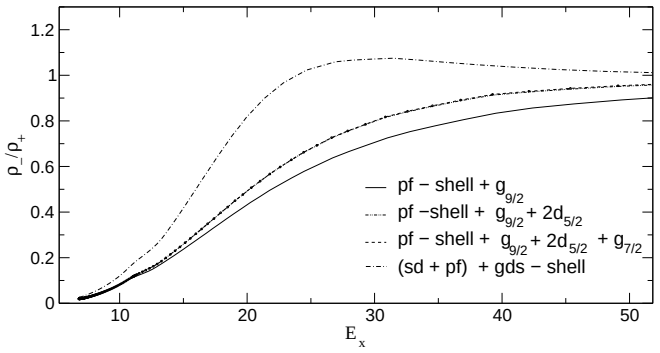

FIG. 2: Ratio of the level densities with odd and even parities as a function of excitation energy $E_{\rm x}$ in MeV in the nucleus ^{56}Fe, calculated with different sizes of the model space. It is evident that it is not sufficient to only include the $pf + g_{9/2}$-shell.

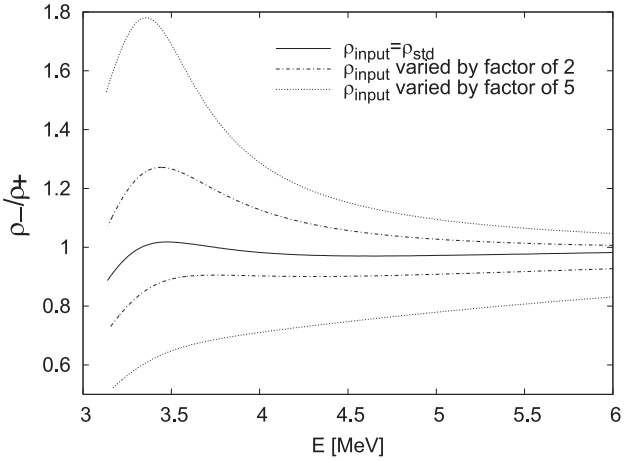

FIG. 3: Influence of a variation of the input level density $\rho_{\rm input}$ on the calculated parity ratios in ^{70}Zn. The full line is obtained by using the standard level density $\rho_{\rm std}$ [2]. The dashed and dotted lines correspond to variations of the input level density by factors 2 and 5, respectively. The s.p. levels are held fixed.

reproduce experimental data well [30, 31]. The same deformation was used as in [2, 32, 33], taken from [16].

Fig. 2 illustrates the dependence of the parity distribution on the single-particle model space in ^{56}Fe. For this nucleus, the addition of the $2d_{5/2}$ orbital to the $pf+g_{9/2}$-shell leads to a deviation over 10% in the parity ratio above excitation energies E_x of about 15 MeV. Further inclusion of higher states such as $1g_{7/2}$ does not change the result for ^{56}Fe (the lines for the results overlap in the figure) but will be important for heavier nuclei. Therefore we had to include all major shells up to 11 $\hbar\omega$.

We also see in Fig. 2 that levels usually considered as inert core can also have an important effect. This is clearly seen in the result accounting for excitations across the full $sd + pf + gds$-shells. Here we find deviations of at least 10% already at $E_x \simeq 7$ MeV and larger deviations at higher excitation energies. This is mainly due to excitations from the sd-shell.

As a further ingredient, a total nuclear level density $\rho_{\rm tot}$ is required in the determination of the total partition function $Z = Z(\beta, \rho_{\rm tot})$. In principle, any total level density determined in any approach could be supplied here. Since we want to apply the derived parity factor to the level density of [2], we took the total level density and the level density parameters from there.

In a fully consistent model, s.p. levels determine the level density assuming all effects have been properly accounted for and provided that the level density can be computed, e.g. in a shell model, for all nuclei at all relevant excitation energies. In principle, this can be achieved, e.g., within the approach of Ref. [1], but is difficult to carry out for a large number of nuclei. For practical purposes it is therefore necessary to include level densities derived in other approaches, such as the shifted Fermi-gas. Proceeding in this manner, however, great care has to be exercised to achieve consistency between the s.p. structure, in our case obtained from the Saxon-Woods model, and the input level density. Inconsistency will lead to spurious effects in the parity ratio as shown in Fig. 3.

Realistically one has to expect that both the s.p. level structure from the Saxon-Woods potential and our total level density bear inherent uncertainties. Thus, when striving for consistency it is anticipated that both inputs should be adapted. Here, we used an iteration method which only varies the level density and not the Saxon-Woods potential, assuming that the s.p. structure is correct. Although this does not limit the applicability of our results, it has to be emphasized that the variation of the level density $\rho_{\rm input} = \rho_{\rm tot}$ shown in Fig. 3 and found in our iteration procedure is not due to the uncertainty of $\rho_{\rm tot}$ alone but rather is supposed to contain the combined uncertainties in $\rho_{\rm tot}$ and the s.p. levels.

In each iteration step the parity projected level-densities

$$\begin{aligned} \rho_g(E) &= \frac{1}{\sqrt{2\pi C^g}}\beta^g \exp(\beta^g E + \ln Z^g) \ , \\ \rho_s(E) &= \frac{1}{\sqrt{2\pi C^s}}\beta^s \exp(\beta^s E + \ln Z^s) \end{aligned} \tag{24}$$

were calculated with an input level density $\rho_{\rm input}$. The total level density in this step is then given by the sum of the parity projections:

$$\rho^{\rm (it)} = \rho_g + \rho_s \ . \tag{25}$$

In the first iteration step the standard level density from Ref. [2] was used for $\rho_{\rm input}$. In each following step, $\rho^{\rm (it)}$ of the previous step became the new $\rho_{\rm input}$ and the procedure continued until $\rho^{\rm (it)}$ and $\rho_{\rm input}$ converged. Convergence was usually achieved quickly, typically in the third iteration step.

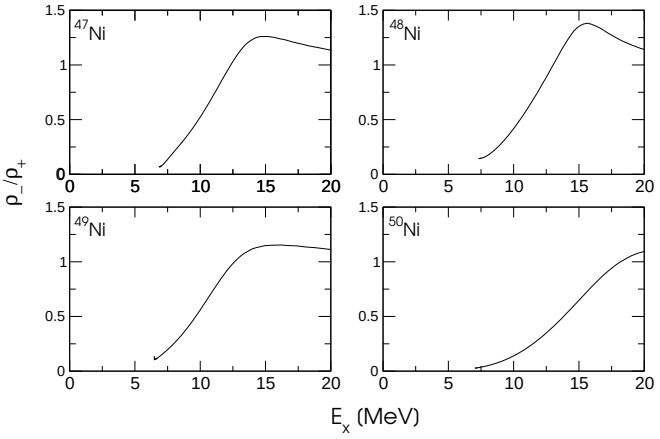

FIG. 4: Ratio of the parity projected level densities as a function of excitation energy for Ni isotopes around the neutron *sd*-shell closure.

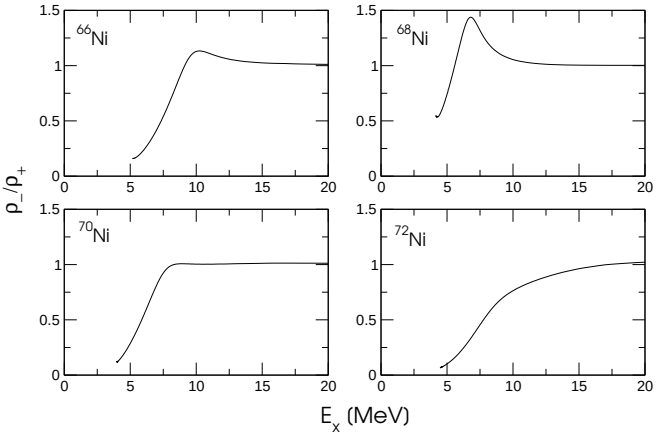

FIG. 5: Ratio of the parity projected level densities as a function of excitation energy for Ni isotopes around the neutron pf-shell closure.

D. Results and discussion of selected examples

Using the approach described in the previous sections, we have calculated ratios of parity-projected level densities for all nuclei from Ne to Bi and from proton dripline to neutron dripline, adopting the large $11\hbar\omega$ model space. All target nuclei in [32, 33] are covered[1]. The results can be obtained from the American Institute of Physics' EPAPS [34] or directly from the authors at `http://nucastro.org`.

Representative for our results are Figs. 4–9. It can immediately be noticed that the parities equilibrate only at excitation energies above about $5-10$ MeV or even higher (see, e.g., Fig. 4), even for the more heavy nuclei. This underlines the importance of using a parity projection factor $\mathcal{P} \neq 1/2$ at most energies of astrophysical interest.

Surprising at first glance is the effect we found at closed shells. The parity ratio can overshoot the equilibrated value of $\rho_s/\rho_g = 1$ by 20–60 % before finally reaching the equilibrium value at higher excitation energies. The overshooting can be understood by the fact that parity can only be changed by excitations between s.p. levels of different parity. When an oscillator shell is completely filled, i.e. the next available subshell exhibits opposite parity, any excitation will change the parity of the system, resulting in a dominance of opposite parity states.

While studying the following examples, it should be kept in mind that both neutron and proton excitations contribute to the parity ratio. When comparing the ratios within an isotopic chain, however, the proton contribution will remain the same and differences between isotopes can be attributed to the change in neutron number. Similar considerations apply to the comparison of isotones and the changing proton number. For example, Fig. 4 shows the evolution of the parity ratio in Ni isotopes around the neutron *sd*-shell closure. The *sd*-shell is filled completely with neutrons for ^{48}Ni. Every excitation of ^{48}Ni populates a single particle level of opposite parity leading to a maximal parity change. The formation of the peak can already be seen for ^{47}Ni but the position of the peak is shifted towards smaller excitation energies. This energy shift is about 1 MeV reflecting the energy that is needed to break a neutron pair prior to excitation. The isotopes ^{49}Ni and ^{50}Ni, which both already populate the pf-shell in neutrons, equilibrate at much higher excitation energies. Parity change can be achieved by excitations to the $g_{9/2}$ shell or by excitations from the sd to the pf shell, requiring higher energy on average than for the preceding isotopes.

The evolution of the parity ratio for Ni isotopes at the interface of the pf and gds shell is shown in Fig. 5. Again, a similar behavior as described above can be observed. The $N = 40$ neutron shell is completely filled for ^{68}Ni. Each excitation from the last occupied $2p_{1/2}$ level with negative parity will populate levels from the gds shell with positive parity resulting in a parity-change of maximal amplitude. The formation of the peak can already be seen for ^{66}Ni. The position of the peak is shifted to higher energies as a larger gap between the $2f_{5/2}$ level and the $g_{9/2}$-level has to be bridged.

The transitions between the same shells as above in Fe isotopes is shown in Fig. 6. Moving from ^{56}Fe, where the neutron pf-shell is only half-filled, to ^{66}Fe, where the $2p_{1/2}$-shell is completely filled, it can be seen that the ratio approaches unity for lower values of the excitation energy as one approaches the $N = 40$ shell closure. As the parity can only be changed by excitations either from the sd to the pdf shell or from the pf to the gds shell, the ratio will equilibrate faster with increasing neutron number as the gap between the last occupied orbit in

[1] It should be noted that this also impacts, for example, the resulting driplines as the same inputs as in these references were used here.

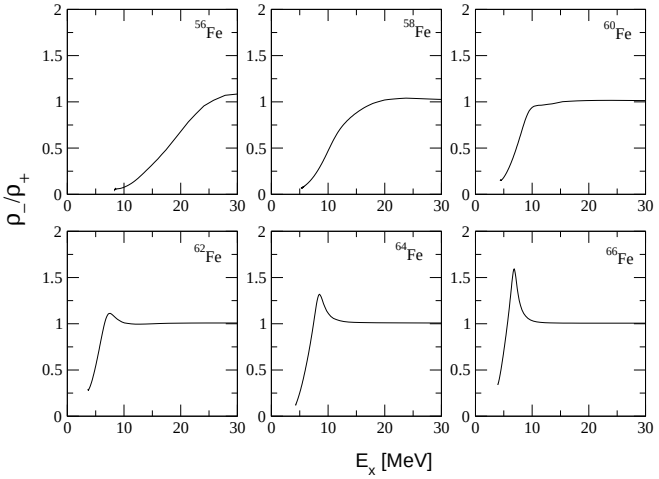

FIG. 6: Ratio of the parity projected level densities as a function of excitation energy for Fe isotopes up to $N = 40$.

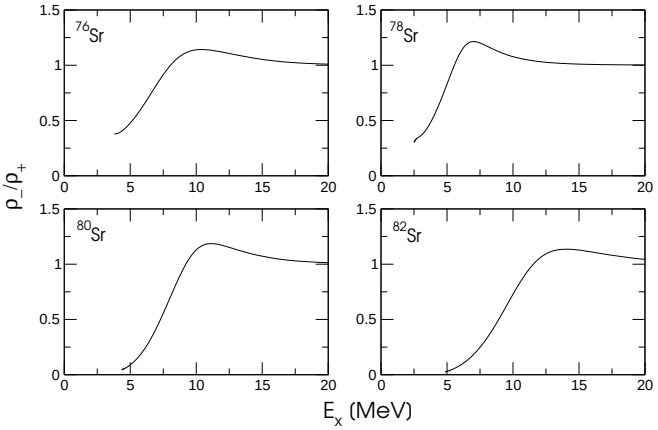

FIG. 7: Evolution of the ratios of the parity projected level densities as a function of excitation energy for Sr isotopes around the neutron pf-shell closure.

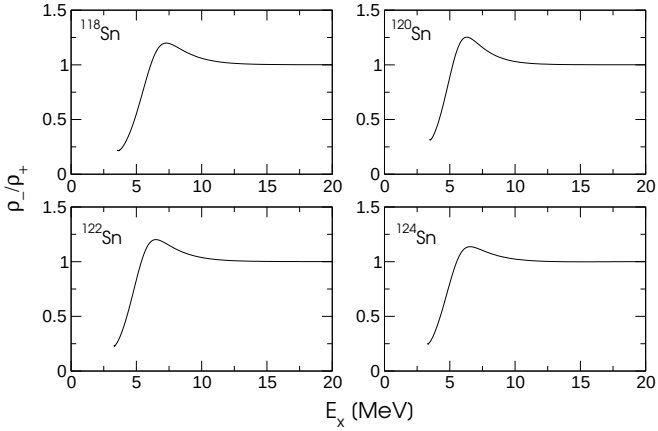

FIG. 8: Evolution of the ratios of the parity projected level densities as a function of excitation energy for Sn isotopes around the neutron gds-shell closure.

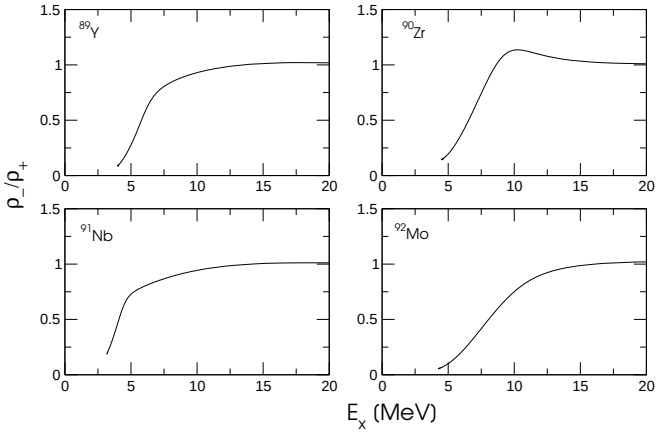

FIG. 9: Evolution of the odd- to even-parity ratio within the $N = 50$ isotones in the vicinity of the proton pf-shell closure.

the pf-shell and the gds-shell will decrease. For ^{66}Fe, where the pf shell is completely filled, a pronounced peak around 8 MeV occurs.

A similar behaviour is illustrated by Fig. 7 for the evolution of the parity ratio in Sr isotopes at the pf and gds interface. Again, the ratio reaches a maximum in ^{78}Sr with the filling of the neutron pf-shell. A comparison to the Fe isotopes with the same neutron numbers in Fig. 6 shows the impact of deformation. The FRDM model [16] predicts the Sr isotopes shown here to be strongly deformed. The resulting level splitting leads to a wider, less pronounced peak in the Sr isotopes as compared to the Fe isotopes.

Another interesting case is seen in Fig. 8 which displays the evolution of the parity ratio in Sn isotopes in the vicinity of the gds- and pfh-shell. The $h_{11/2}$-subshell is half filled at ^{120}Sn due to the fact that it is located below the $2d_{3/2}$ and $3s_{1/2}$-subshells, the latter two belonging to the gds-shell. Comparatively small excitation energy is required to change the parity by either moving neutrons from the $h_{11/2}$-subshell to the higher ds-states or by populating the $h_{11/2}$-subshell with neutrons from lower gd-states. The effect of the latter is largest when the $h_{11/2}$-subshell is least occupied, the effect of the former becomes larger with increased occupation. That is why there is an overshooting peak found in all Sn isotopes shown in Fig. 8, with the one in ^{120}Sn being the most pronounced because both excitations contribute almost equally. However, due to the mixing of gds- and $h_{11/2}$-states, the overshooting is not as strong as the one found for ^{66}Fe at the pf-closure.

Above, the evolution of the parity ratio was discussed in isotopic chains, where each parity change results from an excitation of neutrons only. A similar effect is found for protons. For instance, Fig. 9 shows the evolution of the $N = 50$ isotone parity ratio. The proton numbers for the four shown nuclei (Y, Zr, Nb, and Mo) are 39, 40, 41, and 42, respectively. Again, a peak can be observed in ^{90}Zr as the proton pf-shell is completely filled for this

nucleus. Weak deformation is predicted for these nuclei which leads to a suppression of the peak.

III. APPLICATION IN ASTROPHYSICS

A. Introduction

In the following we discuss the implications of a realistic parity distribution in astrophysical applications. The astrophysical reaction rate is the central quantity in the nuclear reaction networks employed to follow nucleosynthesis in different astrophysical environments. For nucleon-nucleus and nucleus-nucleus reactions it is given by folding the reaction cross section with the Maxwell-Boltzmann velocity distribution of the interacting nuclei

$$r = n_1 n_2 \sqrt{\frac{8}{\pi M \left(kT^*\right)^3}} \int_0^\infty \sigma^*(E') E' \exp\left(-\frac{E'}{kT^*}\right) dE' \,. \tag{26}$$

The stellar plasma temperature is denoted by T^*, the reduced mass of the interacting nuclides by M, and their number densities by n_1, n_2. The stellar cross section is defined as

$$\sigma^*(E_{\rm c.m.}) = \frac{\sum_\mu (2J^\mu + 1) \exp(-E^\mu/kT^*) \sum_\nu \sigma^{\mu\nu}(E_{\rm c.m.})}{\sum_\mu (2J^\mu + 1) \exp(-E_i^\mu/kT^*)} \tag{27}$$

including sums over excited states μ, ν in the target and final nucleus, respectively, with J^μ and E^μ denoting spin and excitation energy of the μ-th target state.

B. Relevant reaction theory

For the majority of reactions relevant in astrophysics, the reaction cross sections $\sigma^{\mu\nu}$ have to be calculated with different reaction models as experimental information often is not available in the relevant energy range or even impossible to obtain due to the short half-lives of the involved nuclei. Even if data is available, it can only provide a measure of $\sigma^\mu = \sum_\nu \sigma^{\mu\nu}$ and thus does not provide the required σ^*. Depending on the number of resonances in the Gamow window [2], one has to consider direct reactions, the influence of few resonances, or an average over many resonances [35]. Here, we want to focus on the latter and on direct capture.

Provided there is a high number of resonances at the relevant interaction energy, the formation and decay of a compound nucleus can be described by averaged transmission coefficients in the statistical model or Hauser-Feshbach formalism [36]. The transmission coefficients describing the decay of a compound state k via a process y – with y usually being emission of nucleons, α particles, or γ quanta – include sums of the type ${}^kT_y^{J^k\pi^k} = \sum_\nu {}^kT_y^{J^k\pi^k \to J^\nu\pi^\nu}$. Depending on the nucleus,

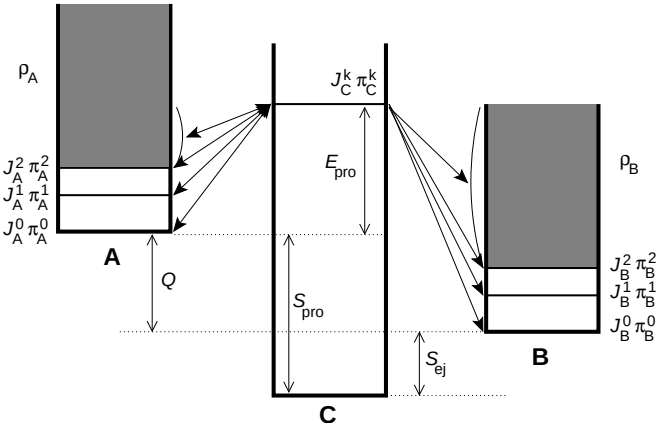

FIG. 10: Energy scheme of a compound nucleus reaction $A + \text{pro} \to C^* \to \text{ej} + B$. For a capture reaction on target nucleus A the ejectile "ej" will be γ radiation and the final nucleus B will be identical to the compound nucleus C. The standard reaction Q value is the difference between the separation energies of the projectile and the ejectile $Q = S_{\rm pro} - S_{\rm ej}$. When considering individual transitions between excited states in the target and the final nucleus the released energy becomes $Q = (S_{\rm pro} + E_A^\mu) - (S_{\rm ej} + E_B^\nu)$, with the excitation energies E_A^μ, E_B^ν. The excitation energy of the accessed compound state is then $E_C^k = S_{\rm pro} + E_{\rm pro} + E_A^\mu$, with $E_{\rm pro}$ being the projectile energy. The decay of the compound state k is computed by a sum of transitions to individual states and by integrating over an average level density (shaded area) above the last included state. The target A can become excited by thermal population of the excited states in an astrophysical plasma.

reaction Q value, and interaction energy $E_{\rm c.m.}$, the properties (spin J^ν, parity π^ν, excitation energy E^ν) of the accessible states may not be known above a certain energy $E_{\rm c}$. Then the sum is replaced by an integration over a level density

$$\begin{aligned} {}^kT_y^{J^k\pi^k} \;=\; & \int_{E_{\rm c}}^{Q+E_{\rm c.m.}} \sum_{J^\nu,\pi^\nu} T_y^{J^k\pi^k \to J^\nu\pi^\nu}(Q + E_{\rm c.m.} - E^\nu) \times \\ & \times \rho(E^\nu, J^\nu, \pi^\nu) dE^\nu \,. \end{aligned} \tag{28}$$

The integration starts from $E_{\rm c} = 0$ in most cases far from stability where no excited states are known. The level density $\rho(E^\nu, J^\nu, \pi^\nu)$ includes the assumption of the parity distribution. It should be noted that this is the level density in the final nucleus which is identical to the compound nucleus only for capture reactions. The interaction energies $E_{\rm c.m.}$ in astrophysics typically are smaller than 1 MeV for neutrons and 5–10 MeV for charged projectiles. A comparison with our results from the previous section shows that the parity ratio obviously has not equilibrated at the relevant excitation energies, even though the reaction Q value has to be added to these energies.

Considering thermal excitation of the target states in the transmission coefficients for the formation of the compound nucleus in state k a relation similar to Eq. (28) can

be derived for the transmission coefficients ${}^kT_{y'}$ connecting target and compound state via a process y', this time inserting the level density in the target nucleus. However, due to the exponential suppression of the population of the excited target states (see Eq. 27) significant contributions to the integral will only stem from the lowest energies.

The central assumption of the Hauser-Feshbach model is that the compound state at energy E^k is highly degenerate. Due to the large number of overlapping resonances, the excited compound nucleus can have any combination of spin and parity. The possible combinations will be weighted by the transmission coefficients ${}^kT_{y'}$ describing the formation process and, e.g., accounting for spin selection rules. However, in principle one has to sum over all compound spins J^k and parities π^k when calculating the statistical model cross section

$$\sigma_{\rm HF}^{y'y} \propto \sum_{J^k\pi^k} \left(2J^k+1\right) \frac{{}^kT_{y'}^{J^k\pi^k}\ {}^kT_{y}^{J^k\pi^k}}{\sum\limits_{z=y,y',\ldots} {}^kT_{z}^{J^k\pi^k}} \,. \qquad (29)$$

The denominator contains a total transmission coefficient for each state $J^k\pi^k$, including all possible deexcitation processes, e.g. emission of protons, neutrons, α particles, and γ quanta. The scheme of a compound nucleus reaction is sketched in Fig. 10.

Direct reactions proceed in a different manner, without formation of an excited compound nucleus. A nucleon or nucleon group is directly transferred from the projectile to the final state without excitation of any other nucleons in the system [35, 37, 38]. This mechanism will dominate at very high interaction energies where the compound nucleus formation is suppressed due to the short interaction timescale and at low energies in the absence of resonances, again suppressing the formation of a compound nucleus. In astrophysics, direct capture is expected to be important close to the driplines because of the low particle separation energies. The cross section $\sigma_{\rm DC}^{\mu\nu}$ for direct capture of a projectile on a target in state μ into a final state ν can be calculated, e.g. in the potential model [35, 37, 38] or in the Lane-Lynn formalism [39]. Again, the total capture cross section is the sum of the contributions of the different transitions to discrete states

$$\begin{aligned}\sigma_{\rm DC}^{\mu}(E_{\rm c.m.}, E^\mu, J^\mu, \pi^\mu) = \\ \sum_\nu C_\nu^2 S_\nu \times \\ \times \sigma_{\rm DC}^{\mu\nu}(Q+E_{\rm c.m.}-E^\nu, J^\mu, \pi^\mu, E^\nu, J^\nu, \pi^\nu)\,, \end{aligned} \qquad (30)$$

with C and S denoting the isospin Clebsch-Gordan coefficient and the spectroscopic factor of the final state, respectively. Because of the importance of direct capture close to the driplines only, the discrete states are usually experimentally unknown and have to be extracted from microscopic calculations. However, it has been shown [40] that the resulting cross section is very sensitive to the predicted properties of the states and that thus different microscopic models yield vastly different results.

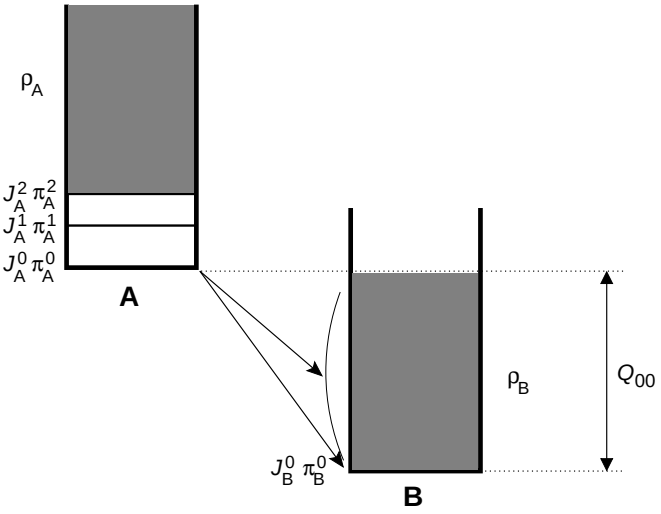

FIG. 11: Energy scheme of a direct capture reaction A+pro $\rightarrow$ $B+\gamma$. The energy of the emitted γ quantum is the energy difference between initial target state and final state. For instance, Q_{00} is the released energy for the ground state to ground state transition and is equal to the binding energy of the projectile in the final nucleus B. As in the case of the compound mechanism, it is possible to include an integration over a level density (shaded region) when the exact properties of the nuclear states are not known. For simplicity, only transitions originating from the ground state of target A are drawn here. For stellar reaction rates it would be important to also include transitions from thermally excited target states.

The sensitivity is much higher than in the case of compound reactions because no averaged quantities are used. In order to circumvent the problem of the exact prediction of the final states it has been suggested [41, 42, 43] to employ averaged properties also for direct captures, i.e. to replace the sum over discrete final states by an integration over a level density

$$\begin{aligned}\bar{\sigma}_{\rm DC}^{\mu} \;=\; & \int_0^Q \sum_{J^\nu,\pi^\nu} \bar{C}^2(E^\nu, J^\nu, \pi^\nu)\bar{S}(E^\nu, J^\nu, \pi^\nu) \times \\ & \times\ \rho(E^\nu, J^\nu, \pi^\nu) \times \\ & \times\ \sigma_{\rm DC}^{J^\mu\pi^\mu\rightarrow J^\nu\pi^\nu}(Q+E_{\rm c.m.}-E^\nu)dE^\nu \end{aligned} \qquad (31)$$

and to use averaged quantities $\bar{C}$ and $\bar{S}$ which are assumed as being constant [43] or energy-dependent [41, 42, 44]. Again, the expression can be extended to include sums over thermally populated target states μ. The situation in the case of a direct capture reaction is shown in Fig. 11.

The sum over spin and parity in Eq. (31) usually contains only few contributing terms because of the dominance of E1 transitions. Because of the small Q values the integration does not include such a large energy range as in the Hauser-Feshbach calculations. These two facts are also the reason why the impact of a non-equilibrated parity ratio will be much larger for direct cross sections than for Hauser-Feshbach ones. The Hauser-Feshbach

model assumes implicitly that the compound nucleus can be formed with any spin and parity (although not with equal probability for each configuration) and that the decay of the compound state by γ- or particle-emission can proceed in transitions to a number of final states. This offers a larger number of possible spin/parity combinations through which the reaction can proceed than in the case of a direct process.

Summarizing, the nuclear level density is important in two aspects. Firstly, to determine the dominant reaction mechanism. Secondly, to calculate cross sections accounting for transitions to a number of final states. It should be noted that these two aspects require the knowledge of the level density at different excitation energies and in different nuclei, the compound nucleus in the former case and the final nucleus in the latter. In the following section III C we study the impact of a changed parity distribution on reaction rates calculated in the two reaction mechanisms described above.

C. Comparison to standard rates and possible implications

1. *Statistical model rates*

Before employing the realistic parity distribution derived in Sec. II in calculations of astrophysical reaction rates, we want to arrive at an estimate of the maximum impact to be expected. The level density enters in the calculation of the transmission coefficient as given by Eq. (28). For the standard assumption of equally distributed parities $\rho(E^\nu, J^\nu, \pi^\nu) = \rho(E^\nu, J^\nu)/2$ for all parities π^ν. As an extreme case we suppose that the parity ratio is Zero at all energies, i.e. only states with the same parity $\pi^0 = \pi^g$ as the ground state occur and $\rho(E^\nu, J^\nu, \pi^\nu) = 0$ for $\pi^\nu \neq \pi^g$. This also implies that $\rho(E^\nu, J^\nu, \pi^g) = \rho(E^\nu, J^\nu)$. We further assume that the formation coefficient ${}^kT_{y'}^{J^k\pi^k}$ dominates the total transmission coefficient in the denominator of Eq. (29) and thus the process y and its transmission coefficients determine the cross section. This can be further simplified by comparing laboratory rates only, i.e. rates with the reaction target being in the ground state.

Two cases can be treated separately, capture reactions and reactions with particle emission, i.e. $y = \gamma$ and $y = \mathrm{n, p}, \alpha, \ldots$, respectively. In the latter case, π^k determines the allowed partial waves in the transition to the state in the final nucleus with π^ν, even partial waves for $\pi^k = \pi^\nu$ and odd partial waves otherwise. For the capture reaction, with π^ν being in the compound nucleus, the parities select the allowed electromagnetic transition, i.e. E1 when $\pi^k \neq \pi^\nu$ and M1 otherwise. For simplicity, electromagnetic transitions with higher order are neglected. For our estimate we also assume that only s- and p-waves contribute to the cross section significantly.

With the above assumptions, the transmission coefficient calculated with Eq. (28) will be comprised of an arithmetic mean between the contributions of the two allowed transitions when taking equidistributed parities. With the restriction of having only one parity available, one of these transitions will be suppressed completely. Therefore, the resulting transmission coefficient will be smaller or larger according to which of the transitions became unavailable. The enhancement factor can be expressed as

$$\mathcal{F}^\uparrow = \frac{2}{1+\chi}\,, \tag{32}$$

the suppression factor is found to be

$$\mathcal{F}^\downarrow = \frac{2\chi}{1+\chi}\,, \tag{33}$$

with $\chi \leq 1$ being the ratio of p- and s-wave transmission coefficient or of M1 and E1 transmission coefficient, respectively,

$$\chi = \begin{cases} \frac{T^{\ell=1}}{T^{\ell=0}} & \text{for particles,} \\ \frac{T^{\mathrm{M1}}}{T^{\mathrm{E1}}} & \text{for radiation.} \end{cases} \tag{34}$$

It can be seen immediately that the enhancement cannot exceed a factor of two even when χ is very small. On the other hand, the suppression can become strong depending on the ratio of the transmission coefficients. Since usually χ is smaller for electromagnetic transitions than for different partial waves of the particles, the largest effects are expected for capture reactions. However, the effect depends on the involved parities. Table I shows the possible combinations.

TABLE I: Enhancement and suppression of transmission coefficients relative to an equal parity distribution.

π	Allowed Transition	Factor
$\pi^k = \pi^\nu$	$\ell = 0$	$\mathcal{F}^\uparrow$
	M1	$\mathcal{F}^\downarrow$
$\pi^k \neq \pi^\nu$	$\ell = 1$	$\mathcal{F}^\downarrow$
	E1	$\mathcal{F}^\uparrow$

An examination of all ratios across the nuclear chart shows that most of them stay in the range given by the above defined $\mathcal{F}^\uparrow$ and $\mathcal{F}^\downarrow$. However, there are several exceptions exhibiting an enhancement of up to a factor of 5. This can be understood by examining the partial widths of the relevant transitions which are directly proportional to the transmission coefficients. In the derivation above it was assumed that the total width is dominated by one of the transitions also appearing in the numerator of Eq. (29) and thus cancelling with the denominator. However, if the total transmission coefficient is dominated by other transitions, e.g. proton- and α-emission in the case of a (n,γ) reaction, then the changes in both T_y and $T_{y'}$ have to be multiplied, leading to an upper limit of a factor of 4. Considering that also the total width

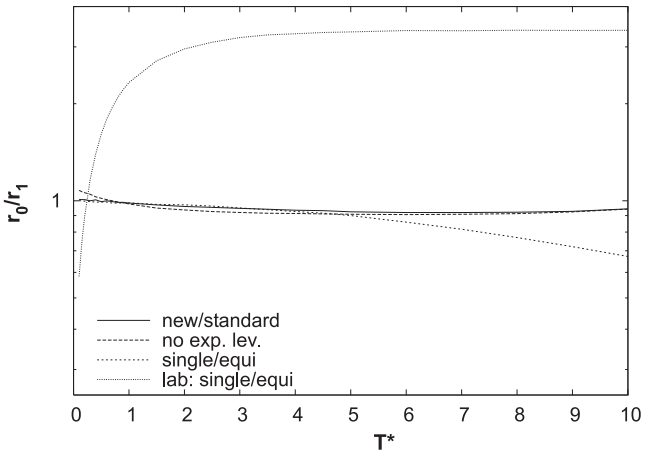

FIG. 12: Ratio of reaction rates as a function of stellar temperature T^* (in 10^9 K) for the reaction ^{67}Se(n,γ)^{68}Se (note the logarithmic scale); the line denoted "lab: single/equi" gives the ratio of laboratory rates with the rate r_0 calculated assuming that only the ground state parity can appear in a nucleus whereas an equal distribution of parities was assumed in rate r_1 and neglecting any experimentally known excited states. Similarly, the ratio of *stellar* rates is plotted as "single/equi". The full line gives the ratio of the "new" stellar rate r_0 calculated with the parity-dependence derived in this work and making use of the level information as given in Table III of Ref. [33] and the "standard" stellar rate r_1 as published in Refs. [32, 33]. For comparison, the ratio obtained without consideration of experimental level information is also plotted as "no exp. lev." (see text).

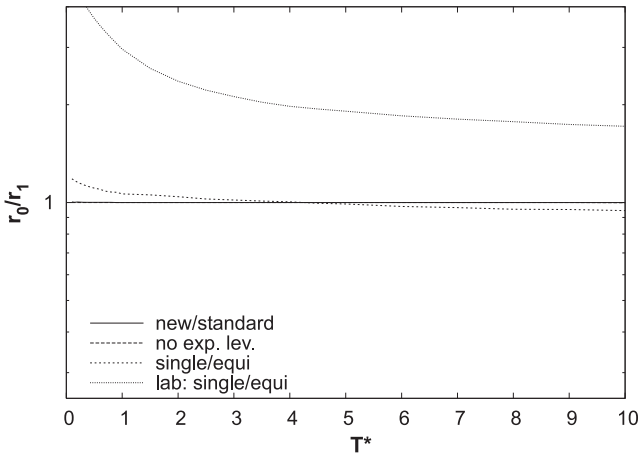

FIG. 13: Same as Fig. 12 but for the reaction ^{68}Se(n,γ)^{69}Se

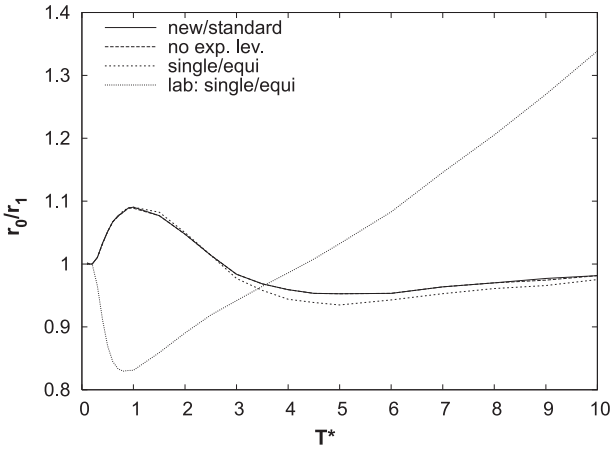

FIG. 14: Same as Fig. 13 but for the reaction ^{68}Se(p,γ)^{69}Se; note the different scale in the figure.

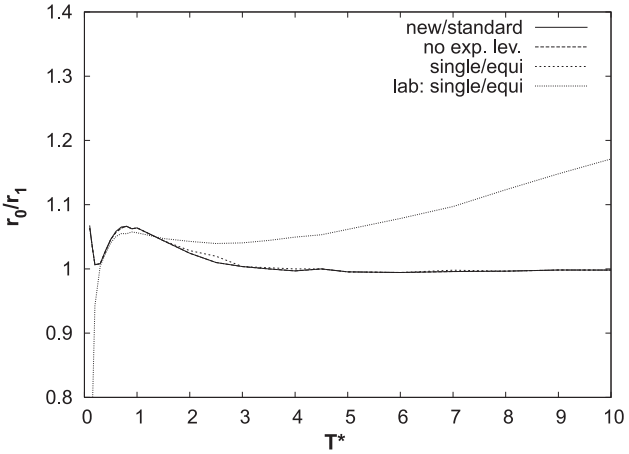

FIG. 15: Same as Fig. 14 but for the reaction ^{67}Se(p,γ)^{68}Se

may be slightly changed, the factor of 5 found in some cases is easily accommodated. Fig. 12 shows the case of ^{67}Se(n,γ) where the neutron width of the compound state k is larger than the γ width but much smaller than both the proton- and α widths. The situation is slightly different for ^{68}Se(n,γ), shown in Fig. 13, where the γ width is much larger than the neutron width but considerably smaller than the proton- and α widths. If the ratio would be fully dominated by one process, then $\mathcal{F}^{\uparrow}$ and $\mathcal{F}^{\downarrow}$ should increase and decrease, respectively, with increasing plasma temperature because at higher excitation energy of the compound nucleus more intermediate levels can be reached. Thus, either more levels can be populated by the preferred transition, giving rise to $\mathcal{F}^{\uparrow}$, or more transitions are missing for $\mathcal{F}^{\downarrow}$. In fact, the total effect stems from an interplay between the stellar temperature dependences of the formation and decay widths (and thus of the enhancement and suppression factors) and their ratios. This can lead to a complicated temperature dependence of the rate ratios with initially declining and finally increasing ratios or vice versa. Examples are shown in Figs. 14 and 15.

The above examples are extreme cases, including a comparison between rates with a parity ratio of zero and rates with equidistributed parities. To show more pronounced effects, no experimentally known levels in the participating nuclei were considered and the targets were

assumed to be in the ground state. For more realistic astrophysical reaction rates, the targets have to be thermally excited according to the plasma temperature which increases the number of possible channels for the formation of the compound nucleus. Moreover, all statistical model calculations consider experimentally determined low-lying states, employing a theoretical level density only above the last included level. This will further reduce the effect of a modified parity distribution but only for nuclei close to stability for which level information is available. Moreover, higher partial waves and multipolarities than considered in the previous estimate will also contribute, thereby further washing out the effects seen above. Figs. 12–15 also show the actual ratio obtained when comparing a full calculation of stellar rates employing the parity distribution derived in Sec. II and including experimental information from Table III of [33] with the standard FRDM rate set published in [32, 33].

2. Direct capture

In principle, Eqs. (32) and (33) also apply for the enhancement and suppression factors, respectively, in the direct capture mechanism. As already mentioned in Sec. III B, however, the transitions allowed by the spin and parity selection rules are more limited than in the compound model and thus the application is more straightforward. Furthermore, there is no energy-dependent renormalization by a total width. Finally, due to the nature of the electromagnetic multipole operators appearing in the expression for the direct capture cross section, E1 radiation is dominating by far and all other multipoles are strongly suppressed (see, e.g., [40]). These factors will lead to a higher sensitivity of direct captures to the parity ratio.

We defer a large-scale calculation of direct capture rates for low capture Q values to another paper but rather want to illustrate the above by a simplified example here. Assuming neutron capture on a $\pi_A = +1$ target state the allowed neutron partial wave ℓ_α in the entrance channel is determined by the parity selection rule

$$(-1)^{\ell_\alpha}\pi_A = (-1)^{\ell_\gamma}\pi_B \quad . \tag{35}$$

Since E1 ($\ell_\gamma = 1$) emission is by far dominating, this can be further simplified to

$$(-1)^{\ell_\alpha} = -\pi_B \quad , \tag{36}$$

with π_B being the parity of the final state. Therefore only even partial waves will be allowed for $\pi_B = -1$ and only odd partial waves for $\pi_B = +1$. The latter relation would just reverse if the target state had odd parity. Because of the low projectile energies relevant in nuclear astrophysics, only s- and p-waves will have a significant contribution to the cross section. Thus, the ratio χ to be inserted in Eqs. (32) and (33) becomes

$$\chi = \frac{\sigma_{\rm DC}^{\mu\to\nu,\text{p-wave}}}{\sigma_{\rm DC}^{\mu\to\nu,\text{s-wave}}} \quad , \tag{37}$$

with $\chi < 1$ because of the higher s-wave cross section ($\sigma_{\rm s} \propto 1/\sqrt{E}$) at small energy. Because of the limited availability of alternative transitions, contrary to the Hauser-Feshbach case the suppression or enhancement cannot be compensated in a direct reaction and the factors $\mathcal{F}^\uparrow$ and $\mathcal{F}^\downarrow$ will have their full effect on each transition. For example, $\chi = 0.18$ for capture of a 100 keV neutron on the 0^+ ground state of ^{140}Sn and ending in a final 3/2 state with an energy release of 1 MeV (see also [40]). The inclusion of thermally populated target states will slightly reduce the effect by making available states with different spin but same parity because of a predominant parity at low excitation energy. This will have a smaller impact than in the Hauser-Feshbach model since low partial waves dominate the cross section, there is no moderating effect of a total width, and generally fewer possible transitions.

TABLE II: Enhancement and suppression of transmission coefficients relative to an equal parity distribution for direct capture on a target state with parity π_A^μ and ending in a final state with parity π_B^ν. The factors $\mathcal{F}^\uparrow$ and $\mathcal{F}^\downarrow$ are defined in Eqs. (32) and (33), respectively.

π	Allowed Transition	Factor
$\pi_A^\mu = \pi_B^\nu$	$\ell_\alpha = 1, 3, 5, \ldots$	$\mathcal{F}^\downarrow$
$\pi_A^\mu \neq \pi_B^\nu$	$\ell_\alpha = 0, 2, 4, \ldots$	$\mathcal{F}^\uparrow$

The application rule for $\mathcal{F}^\uparrow$ and $\mathcal{F}^\downarrow$ for direct capture is shown in Tab. II. For the case of the final nucleus in a capture reaction having opposite parity than the target ground state, the capture rate will be enhanced relative to a rate calculated using a level density with equally distributed parities because of the predominance of states with ground state parity at low excitation energies. This may only be altered if an overshooting of the opposite parity occurs, as discussed in Sec. II D. However, direct capture is important only at such low separation energies that the overshooting regime is not reached.

3. Discussion

We have calculated parity distributions for all nuclei between proton and neutron dripline from Ne to Bi and recomputed the Hauser-Feshbach astrophysical reaction rates given in [32, 33] with the same parameters as quoted there (set FRDM). Selected examples were already shown in Figs. 12–15. In Sec. III C 1 we discussed considerable enhancement or suppression for certain transitions. In the astrophysical context, however, the impact of the new parity ratio remains limited. This is due to several reasons.

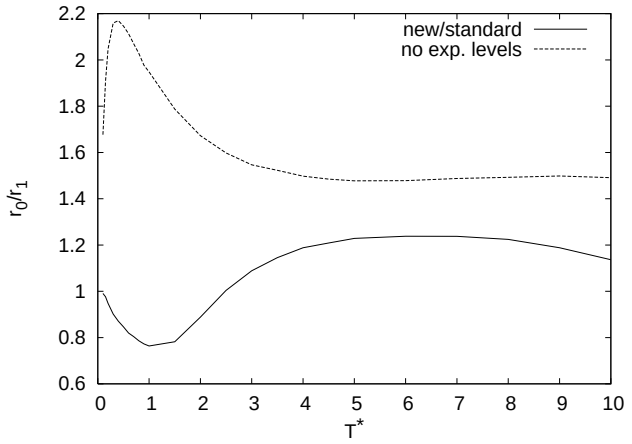

FIG. 16: Stellar reaction rate ratios for ^{94}Nb(p,γ)^{95}Mo as function of stellar temperature T^* (in units of 10^9 K); plotted is the ratio of the stellar rate r_0 calculated with the parity distribution derived in this work with the standard rate r_1 from [32, 33]. Further plotted is the ratio of the same rates but without inclusion of experimentally known low-lying levels (see text).

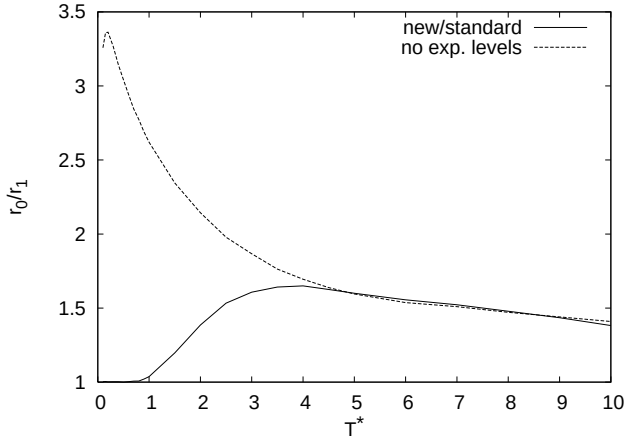

FIG. 17: Same as Fig. 16 but for the reaction ^{95}Zr(p,γ)^{96}Nb

Firstly, the impact of a change in the parity distribution is higher for reactions with large Q values because a larger number of transitions from the compound nucleus is energetically accessible. For example, neutron captures will be altered more strongly on the proton-rich side whereas capture on neutron-rich targets – provided the compound reaction mechanism is dominating – will be less affected. A similar observation can be made for proton capture. Thus, the proton captures occuring in the *rp* process [45, 46] and the neutron captures in the *r* process [47, 48, 49, 50] show changes of several percent relative to the rates computed with an equal distribution of parities.

Moreover, for small capture Q values, the statistical model will not be applicable and resonant or direct capture will dominate. We expect a larger impact of the parity distribution in the averaged direct capture model but further conclusions have to await the recalculation of the direct rates. Even with changed rates, however, it has to be kept in mind that the processes occurring close to the driplines are often in equilibrium, where individual rates are not important to determine the produced nuclear abundances [51]. Rates will only become important in the freeze-out phases when the nucleosynthesis path moves closer to stability [45, 49, 51]. In these phases the compound mechanism will set in again.

Close to the valley of stability level schemes are known to comparatively high excitation energies and are used in the calculations of the relevant nuclear cross sections. Usually, up to 20 levels are included whenever known [32, 33]. This will further reduce the effect of the applied parity distribution because an effective, non-equilibrated parity distribution is already in use for the lowest excitation energies. Figs. 12–15 show a comparison of rates with and without included experimental level information. It should be noted that the slight change in ^{67}Se(n,γ) is not due to neglected levels in ^{68}Se but rather due to the modified transmission coefficients in the competing channels, i.e. proton- and α emission. In the example shown in Figs. 16 and 17, 20 low-lying levels have been considered in all channels in the standard calculation. Removing them, the impact of the parity distribution when using pure level densities can be seen. Generally, only few low-lying states have to be included because the transitions with the highest relative energy, leading to the lowest states, dominate in all channels. Due to the inclusion of experimental information in the standard calculations, the impact of a changed parity distribution is also small for the late freeze-out phases and the nucleosynthesis phases involving nuclei close to the valley of stability. This includes the photodisintegration reactions in *p*-process nucleosynthesis [52, 53, 54], even though they occur on a longer timescale than any freeze-out process.

Finally, the most important mechanism suppressing the impact of the parity distribution is the necessity to include transitions on excited states in the target. In an astrophysical plasma, excited states can be thermally populated as specified in Eq. (27). Because of the Bohr independence hypothesis for compound reactions this allows for a large number of alternative transitions in case one of the parities is suppressed. Small alterations of the energy-dependence of the cross sections cannot be seen in the astrophysical reaction rates anymore due to the folding with the Maxwell-Boltzmann energy distribution of the interacting nuclei according to Eq. (26). The fact that the impact of the parity dependence is strongly suppressed in *stellar* rates can be clearly seen in Figs. 12–17. The larger the stellar temperature, the smaller the parity impact.

Concluding, inclusion of the parity distribution in this work leads to a change in *stellar* reaction rates of only several percent up to about 10% in astrophysically relevant reactions. A few cases exhibit changes up to a factor

of 2 or 1/2, respectively, but are not astrophysically important.

IV. SUMMARY

We generalized a method to calculate the excitation-energy dependent parity distribution in nuclei and used it to calculate parity ratios for all nuclei up to Bi. We demonstrated the importance of including a sufficiently large single-particle model space. In particular, excitations from core single-particle states can also be important. The parity ratio proved to be non-equilibrated up to 5–15 MeV. Interestingly, an overshooting effect in the parity ratio was found at major shell closures where states with ground-state parity are outnumbered by states of opposite parity over a range of several MeV.

The derived parity distribution was then used to recalculate astrophysical reaction rates. The impact of the new description on stellar rates including thermal excitations of the target proved to be limited in the Hauser-Feshbach model although the impact on direct capture has to be studied further.

Acknowledgments

This work was supported in part by the Swiss Nationalfonds (grants 2124-055832, 2000-061031, 2000-105328) and by the U.S. DOE (grant DE-FG-0291-ER-40608).

[1] Y. Alhassid, G. F. Bertsch, and L. Fang, *Phys. Rev. C* **68**, 044322 (2003).
[2] T. Rauscher, F.-K. Thielemann, and K.-L. Kratz, *Phys. Rev. C* **56**, 1613 (1997).
[3] C.E. Rolfs and W.S. Rodney, *Cauldrons in the Cosmos* (University of Chicago Press, Chicago 1988).
[4] B. A. Brown, *Prog. Part. Nucl. Phys.* **47**, 517 (2001).
[5] M. Horoi, J. Kaiser, and V. Zelevinsky, *Phys. Rev. C* **67**, 054309 (2003).
[6] M. Horoi, M. Ghita, and V. Zelevinsky, *Phys. Rev. C* **69**, 041307(R) (2004).
[7] D. J. Dean, S. E. Koonin, K. Langanke, P. B. Radha, and Y. Alhassid, *Phys. Rev. Lett.* **74**, 2909 (1995).
[8] H. Nakada and Y. Alhassid, *Phys. Rev. Lett.* **79**, 2939 (1997).
[9] Y. Alhassid, S. Liu, and H. Nakada, *Phys. Rev. Lett.* **83**, 4265 (1999).
[10] H. A. Bethe, *Phys. Rev.* **50**, 332 (1936).
[11] A. Gilbert and A. G. W. Cameron, *Can. J. Phys.* **43**, 1446 (1965).
[12] K. Langanke, *Nucl. Phys.* **A778**, 233 (2006).
[13] A. P. Zuker, *Phys. Rev. C* **64**, 021303(R) (2001).
[14] P. Van Isacker, *Phys. Rev. Lett.* **89**, 262502 (2002).
[15] T. Rauscher, *Astrophys. J. Suppl. Ser.* **147**, 403 (2003).
[16] P. Möller, J. R. Nix, W. D. Myers, and W. D. Swiatecki, *Atomic Data Nucl. Data Tables* **59**, 185 (1995).
[17] Y. Alhassid, G. F. Bertsch, S. Liu, and H. Nakada, *Phys. Rev. Lett.* **84**, 4313 (2000).
[18] D. Mocelj, T. Rauscher, G. Martínez-Pinedo, and Y. Alhassid, in *Capture γ-Ray Spectroscopy and Related Topics, CGS11*, eds. J. Kvasil, P. Cejnar, M. Krtička (World Scientific, Singapore 2003), p. 781.
[19] D. Mocelj, T. Rauscher, G. Martínez-Pinedo, and Y. Alhassid, *Nucl. Phys.* **A718**, 650c (2003).
[20] D. Mocelj, T. Rauscher, K. Langanke, G. Martínez-Pinedo, L. Pacearescu, A. Faessler, and F.-K. Thielemann, *Nucl. Phys.* **A758**, 154c (2005).
[21] D. Mocelj, T. Rauscher, F.-K. Thielemann, G. Martínez-Pinedo, K. Langanke, L. Pacearescu, and A. Faessler, *J. Phys. G* **31**, S1927 (2005).
[22] D. Mocelj, PhD thesis, University of Basel, Switzerland (2006).
[23] J. Bardeen, L. N. Cooper, and J. R. Schrieffer, *Phys. Rev.* **108**, 1175 (1957).
[24] S. Liu and Y. Alhassid, *Phys. Rev. Lett.* **87**, 022501 (2001).
[25] K. Kaneko and M. Hasegawa, *Phys. Rev. C* **72**, 024307 (2005).
[26] H. Chen and Y. Alhassid, in preparation (2007).
[27] K. Langanke, D. J. Dean, P. B. Radha, and S. E. Koonin, *Nucl. Phys.* **A602**, 244 (1996).
[28] J. Damgaard, H. C. Pauli, V. V. Pashkevic, and V. M. Sturinski, *Nucl. Phys.* **A135**, 432 (1969).
[29] Y. Tanaka, Y. Oda, F. Petrovich, and R. K. Sheline, *Phys. Lett. B* **83**, 279 (1979).
[30] R. Nojarov, A. Faessler, P. Sarriguren, E. Moya de Guerra, and M. Grigorescu, *Nucl. Phys.* **A563**, 349 (1993).
[31] P. Sarriguren, E. Moya de Guerra, R. Nojarov, and A. Faessler, *J. Phys. G* **19**, 291 (1993).
[32] T. Rauscher and F.-K. Thielemann, *Atomic Data Nucl. Data Tables* **75**, 1 (2000).
[33] T. Rauscher and F.-K. Thielemann, *Atomic Data Nucl. Data Tables* **79**, 47 (2001).
[34] See EPAPS Document No. E-PRVCAN-75-013705 for the calculated parity ratios as function of excitation energy. For more information on EPAPS, see `http://www.aip.org/pubservs/epaps.html`.
[35] P. Descouvement and T. Rauscher, *Nucl. Phys.* **A777**, 137 (2006).
[36] W. Hauser and H. Feshbach, *Phys. Rev.* **87**, 366 (1952).
[37] G. R. Satchler, *Direct Nuclear Reactions*, Clarendon Press (Oxford, 1983).
[38] N. K. Glendenning, *Direct Nuclear Reactions*, Academic Press (New York, 1983).
[39] A. M. Lane and E. Lynn, *Nucl. Phys.* **17**, 563 (1960); **17**, 586 (1960).
[40] T. Rauscher, R. Bieber, H. Oberhummer, K.-L. Kratz, J. Dobaczewski, P. Möller, and M. M. Sharma, *Phys. Rev. C* **57**, 2031 (1998).
[41] T. Rauscher, report IKP1996-02017, TU Wien (1996).
[42] E. Holzer, *Statistische Berechnung von direktem Neutroneneinfang*, Master thesis, TU Wien (1997).
[43] S. Goriely, *Astron. Astrophys.* **325**, 414 (1997).
[44] R. Ejnisman, I.D. Goldman, K.S. Krane, P. Mohr, Y. Nakazawa, E.B. Norman, T. Rauscher, and J. Reel, *Phys.*

Rev. C **58**, 2531 (1998).
[45] H. Schatz *et al.*, *Phys. Rep.* **294**, 167 (1998).
[46] H. Schatz, A. Aprahamian, V. Barnard, L. Bildsten, A. Cumming, M. Ouellette, T. Rauscher, F.-K. Thielemann, and M. Wiescher, *Phys. Rev. Lett.* **86**, 3471 (2001).
[47] J. J. Cowan, F.-K. Thielemann, and J. W. Truran, *Phys. Rep.* **208**, 267 (1991).
[48] Y.-Z. Qian and S. E. Woosley, *Astrophys. J.* **471**, 331 (1996).
[49] C. Freiburghaus, J.-F. Rembges, T. Rauscher, E. Kolbe, F.-K. Thielemann, K.-L. Kratz, B. Pfeiffer, and J. J. Cowan, *Astrophys. J.* **516**, 381 (1999).
[50] B. Meyer, *Astrophys. J.* **343**, 254 (1989).
[51] T. Rauscher, *Nucl. Phys.* **A758**, 655c (2005).
[52] S. E. Woosley and W. M. Howard, *Astrophys. J. Suppl. Ser.* **36**, 285 (1978).
[53] M. Rayet, N. Prantzos, and M. Arnould, *Astron. Astrophys.* **227**, 271 (1990).
[54] M. Arnould and S. Goriely, *Phys. Rep.* **384**, 1 (2003).